Robotica (2015) volume 33, pp. 1231–1249. © Cambridge University Press 2014
doi:10.1017/S0263574714000654

# An efficient approach to pose tracking based on odometric error modelling for mobile robots

Jingdong Yang†*, Jinghui Yang‡ and Zesu Cai§

†*School of Optical-Electrical and Computer Engineering, Shanghai Key Lab of Modern Optical System, University of Shanghai for Science and Technology, Shanghai 200093, China;*
‡*School of Business Management, Shanghai Second Polytechnic University, Shanghai 201209, China;*
§*Department of Computer Science and Technology, Harbin Institute of Technology, Harbin 150001, China*

(Accepted February 17, 2014. First published online: April 1, 2014)

**SUMMARY**
Odometric error modelling for mobile robots is the basis of pose tracking. Without bounds the odometric accumulative error decreases localisation precision after long-range movement, which is often not capable of being compensated for in real time. Therefore, an efficient approach to odometric error modelling is proposed in regard to different drive type mobile robots. This method presents a hypothesis that the motion path approximates a circular arc. The approximate functional expressions between the control input of odometry and non-systematic error as well as systematic error derived from odometric error propagation law. Further an efficient algorithm of pose tracking is proposed for mobile robots, which is able to compensate for the non-systematic and systematic error in real time. These experiments denote that the odometric error modelling reduces the accumulative error of odometry efficiently and improves the specific localisation process significantly during autonomous navigation.

KEYWORDS: Extended Kalman filter; Odometric error modelling; Non-systematic error covariance; Pose estimate; Global localisation.

## 1. Introduction

The odometric error includes systematic error and non-systematic error for mobile robots, the former relates to the structural error, which can be reduced by inner calibration. The later denotes a random error caused by the disturbance of external or internal factors to movement.[1–4] Being the main elements which degrade localisation precision, these factors have great influence on the pose estimate of robots in the process of pose tracking. The reduction of odometric error and improvement of localisation precision have become the focus of study of mobile robots.[5,6]

Chong assumed that robots move along circular arcs, analysed non-systematic error in a theoretical way and computed odometric errors covariance matrices.[7,8] He considered the travel distance of left wheel and right wheel as an odometric input. However, the velocity and angular velocity are often regarded as the input of the odometry to describe the movement in some larger environment. Chong's method only applies to a synchronous-drive mobile robot, and does not apply to other drive robots. Martinelli presented an odometric error modelling for synchronous drive platform and a possible strategy for evaluating the odometric error.[9,10] He used three axes to express the relations of position and direction, and introduced the observer value and projection axis to maximize the accuracy on the parameter estimation reachable with these observables. Though the simulation tests have been carried out for a synchronous drive and a differential drive robot, the error modelling approach is just applicable to a real differential-drive robot and cannot be applied to other drive mobile robots practically. In addition, he did not give the derivation and proof concerning odometry error modelling

* Corresponding author. E-mail: eerfriend@126.com

https://doi.org/10.1017/S0263574714000654 Published online by Cambridge University Press

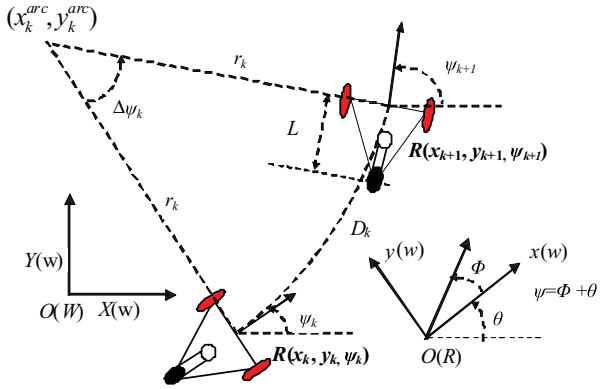



Fig. 1. The odometric kinematic model for mobile robots.

in detail. A closed-form expression of the covariance matrix of position uncertainty is proposed for a non-holonomic Ackerman driving-type of autonomous vehicles.[11,12] The approach can form a general expression for the covariance matrix of pose estimation. However, it is only compatible to non-holonomic Ackerman driving-type robots rather than a general error modelling platform for mobile robots. Reference [1] addresses the odometry error modelling including systematic error and non-systematic error, but does not give the detailed derivation. The proposed error modelling is not applied to practical pose tracking either.

This paper proposes a general odometric error modelling for both differential drive and synchronous-drive mobile robots. Further, the modelling with odometric error feedback in real time is applied to pose tracking during autonomous navigation for mobile robots. In the end, the experiments justify the practicability and robustness of the odometry error modelling.

## 2. Odometry Model

An odometric error platform with high performance involves the kinematics of mobile robots. Different drive types of mobile robots demand different kinematic models of odometry. In this section, a general odometric model is proposed for differential drive and synchronous drive mobile robots.

We assume that the motion path is a circular arc which is shown in Fig. 1. The path from pose $s_k$ to pose $s_{k+1}$ is considered as a section of an arc with radius $r_k$. $O(R)$, is the robot coordinates. In the world coordinates, $O(W)$, the coordinate of the arc centre is $(x_k^{arc}, y_k^{arc})$, and the robot pose is $(x(w), y(w), \psi)$,$\psi = \theta+\varphi$, where $\psi$ is the arc angle of arc motion, $\theta$ is the orientation angle, and the steer angle $\varphi$ denotes the intersection angle between the front wheel and the centre axis, which manoeuvres robot turn in motion. Introduce $\nabla\psi$ as the direction change of motion from one step to the next

$$\psi_{k+1} = \psi_k + \nabla\psi_k.$$

According to the kinematic principle, the relations between any two poses $(x_k, y_k)$ and $(x_{k+1}, y_{k+1})$ can be described as follows:

$$\begin{cases} x_k = x_k^{\text{arc}} + r_k \cos\left(\psi_k - \frac{\pi}{2}\right) = x_k^{\text{arc}} + r_k \sin\psi_k \\ y_k = y_k^{\text{arc}} + r_k \sin\left(\psi_k - \frac{\pi}{2}\right) = y_k^{\text{arc}} - r_k \cos\psi_k \end{cases} \quad \text{and}$$

$$\begin{cases} x_{k+1} = x_k^{\text{arc}} + r_k \cos\left(\psi_{k+1} - \frac{\pi}{2}\right) = x_k^{\text{arc}} + r_k \sin\psi_{k+1} \\ y_{k+1} = y_k^{\text{arc}} + r_k \sin\left(\psi_{k+1} - \frac{\pi}{2}\right) = y_k^{\text{arc}} - r_k \cos\psi_{k+1}. \end{cases}$$

So the robot pose at time $k+1$ is easily identified as a function of the pose at time $k$

$$\begin{cases} x_{k+1} = x_k + r_k(\sin\psi_{k+1} - \sin\psi_k) \\ y_{k+1} = y_k - r_k(\cos\psi_{k+1} - \cos\psi_k). \end{cases} \tag{1}$$

Let $u_k = (D_k, \nabla\psi_k)$ be the input of the odometry model, where $D_k$ is the distance travelled along the curve and $\nabla\psi_k$ is the change in motion direction. Supposing when the direction of rotation is

https://doi.org/10.1017/S0263574714000654 Published online by Cambridge University Press

clockwise, $r_k$ is negative, otherwise, $r_k$ is positive

$$r_k = \frac{D_k}{\Delta\psi_k}. \tag{2}$$

So, the robot pose $s_{k+1}$ at time $k+1$ can be expressed as the non-linear function of the pose $s_k$ at time $k$, the control input $u_k$ and the noise $w_k$

$$s_{k+1} = f(s_k, u_k, w_k, \Delta\psi_k) = \begin{pmatrix} x_k + r_k(\sin(\psi_k + \Delta\psi_k) - \sin\psi_k) \\ y_k - r_k(\cos(\psi_k + \Delta\psi_k) - \cos\psi_k) \\ \psi_k + \Delta\psi_k \end{pmatrix}$$
$$= \begin{pmatrix} x_k + \frac{D_k}{\Delta\psi_k}(\sin(\psi_k + \Delta\psi_k) - \sin\psi_k) \\ y_k - \frac{D_k}{\Delta\psi_k}(\cos(\psi_k + \Delta\psi_k) - \cos\psi_k) \\ \psi_k + \Delta\psi_k \end{pmatrix}.$$

## 3. Odometric Non-Systematic Error Analysis

The non-systematic error refers to the uncertain error and is often characterized by error mean and error covariance. In most cases, the error mean approximates zero after calibration and is often excluded. Therefore, the research on non-systematic error covariance has become the main aspect of research on non-systematic error. In the rest of this paper, we use the notation $\nabla_{s_k} f = \nabla_{s_k}$, $\nabla_{u_k} f = \nabla_{u_k}$ to denote the Jacobian of $f(s_k, u_k)$ with respect to $s_k$ and $u_k$, and use $c$ and $s$ to denote cosine and sine in the following equation, respectively.

**Assumption 1.** The covariance matrix of non-systematic error $Q_k$ is made up of the sum of $Q_k^i$ when $N \to \infty$

$$Q_k = \sum_{i=0}^{N-1} Q_k^i. \tag{3}$$

**Assumption 2.** $C_{u_k}$, the covariance matrix of odometric input $u_k$ is assumed to be diagonal matrix

$$C_{u_k} = \begin{bmatrix} \delta_{D_k}^2 & 0 \\ 0 & \delta_{\psi_k}^2 \end{bmatrix}, \tag{4}$$

where $\delta_{D_k}^2$ is the variance in distance travelled and $\delta_{\psi_k}^2$ is the variance in change in motion direction.

The error caused by the correlation among the parameters is not discussed here. It is assumed that $\delta_{D_k}^2$ depends solely on the distance travelled $D_k$. $\delta_{\Delta\psi_k}^2$ depends on both distance travelled $D_k$ and the change in motion direction $\nabla\psi_k$, so the following equations can be given

$$\delta_{D_k}^2 = k_D \left| D_k \right| = k_D \left| r_k \Delta\psi_k \right|, \tag{5}$$

$$\delta_{\Delta\psi_k}^2 = k_\psi^\psi \left| \Delta\psi_k \right| + k_\psi^D \left| D_k \right| = \left( k_\psi^\psi + k_\psi^D \left| r_k \right| \right) \left| \Delta\psi_k \right| = k_\psi \left| \Delta\psi_k \right|, \tag{6}$$

where $k_D, k_\psi, k_\psi^\psi, k_\psi^D$ are constants referring to uncertain empirical parameters between the ground and the wheels.

The pose estimate $s_{k+1}$ is a Markov process which only has a connection with the pose estimate at time $k$. To deduce the error covariance of $s_{k+1}$, we assume that first-order Taylor's expansion does not introduce significant higher order error, and the pose error at time $k$ is not correlated with the input error of odometry $P_{k+1}$.The covariance matrix of $s_{k+1}$ can be deduced on the basis of Assumption 1 and Assumption 2[13,14]

$$P_{k+1} = (\nabla s_k) P_k (\nabla s_k)^T + (\nabla u_k) C_{u_k} (\nabla u_k)^T = (\nabla s_k) P_k (\nabla s_k)^T + Q_k, \tag{7}$$

https://doi.org/10.1017/S0263574714000654 Published online by Cambridge University Press

where the two Jacobian matrices in (7) are given as follows:

$$\nabla s_k = \begin{pmatrix} 1 & 0 & r_k(c\psi_{k+1} - c\psi_k) \\ 0 & 1 & r_k(s\psi_{k+1} - s\psi_k) \\ 0 & 0 & 1 \end{pmatrix}, \tag{8}$$

$$\begin{aligned} \nabla u_k &= \begin{pmatrix} \frac{1}{\Delta\psi_k}(s\psi_{k+1} - s\psi_k) & -\frac{D_k}{(\Delta\psi_k)^2}(s\psi_{k+1} - s\psi_k) + \frac{D_k}{\Delta\psi_k}c\psi_{k+1} \\ -\frac{1}{\Delta\psi_k}(c\psi_{k+1} - c\psi_k) & \frac{D_k}{(\Delta\psi_k)^2}(c\psi_{k+1} - c\psi_k) + \frac{D_k}{\Delta\psi_k}s\psi_{k+1} \\ 0 & 1 \end{pmatrix} \\ &= \begin{pmatrix} \frac{1}{\Delta\psi_k}(s\psi_{k+1} - s\psi_k) & -\frac{r_k}{\Delta\psi_k}(s\psi_{k+1} - s\psi_k) + r_k c\psi_{k+1} \\ -\frac{1}{\Delta\psi_k}(c\psi_{k+1} - c\psi_k) & \frac{r_k}{\Delta\psi_k}(c\psi_{k+1} - c\psi_k) + r_k s\psi_{k+1} \\ 0 & 1 \end{pmatrix}. \end{aligned} \tag{9}$$

**Lemma 1.** Assume that the odometric error at time $k$ is not correlated with the input error of odometry, then the covariance matrix of odometry non-systematic error at time $k$ can be expressed by the function of the control input of odometry:

$$Q_k = g(r_k, \Delta\psi_k, \psi_k, \psi_{k+1}, D_k, k_D, k_\psi, k_\psi^\psi, k_\psi^D).$$

**Proof 1. Circular arc motion**

Supposing the mobile robot is a mass point during autonomous exploration in a larger environment, some researches will be simplified and is applied on differential drive robots, synchronous drive types, etc. If the movement of the robot is divided into infinite steps, and the odometric error covariance of each step is described by the input of odometry, the accumulative odometric error can be expressed by the limit sums of infinitude function.

Now divide the $k$th step into $N$ sub-steps, $i = 1,\ldots, N$, such as $s_k^0 = s_k$ and $s_k^N = s_{k+1}$ as well as $P_k^0 = P_k$ and $P_k^N = P_{k+1}$. According to the above analysis, Equation (7) can be written as follows:

$$P_{k+1} = P_k^N = (\nabla s_k^{N-1})P_k^{N-1}(\nabla s_k^{N-1})^T + (\nabla u_k^{N-1})C_{u_k}^{N-1}(\nabla u_k^{N-1})^T. \tag{10}$$

The recursive expansions of $P_k^i$ and $C_{u_k}^i$ of Equation (10) goes as follows:

$$P_{k+1} = \left(\prod_{i=0}^{N-1}\nabla s_k^i\right) P_k \left(\prod_{i=0}^{N-1}\nabla s_k^i\right)^T + \sum_{i=0}^{N-1}\left[\left(\prod_{j=i+1}^{N-1}\nabla s_k^j\right)\nabla u_k^i C_{u_k}^i \left(\nabla u_k^i\right)^T \left(\prod_{j=i+1}^{N-1}\nabla s_k^j\right)^T\right]. \tag{11}$$

The following equation, according to Equation (8), can be obtained:

$$\prod_{j=i+1}^{N-1}\nabla s_k^j = \begin{pmatrix} 1 & 0 & r_k\left(c\psi_k^{N-1} - c\psi_k^{i+1}\right) \\ 0 & 1 & r_k\left(s\psi_k^{N-1} - s\psi_k^{i+1}\right) \\ 0 & 0 & 1 \end{pmatrix}. \tag{12}$$

To analyse $Q_k^i$, start with the second term of Equation (11). The path travelled between time $k$ and $k+1$ is split into infinitesimal small segments. When $N\to\infty, \Delta\psi_k^i \to 0$ for each small segment and $\psi_k^{N-1} \to \psi_{k+1}$. The extended error between the step $N$ and the step $N$-1 also approaches zero approximately, when $N\to\infty$. Based on the following equations:

$$\lim_{\varepsilon\to 0}(\sin(\alpha+\varepsilon) - \sin(\alpha)) = \varepsilon\cos\alpha, \tag{13}$$

$$\lim_{\varepsilon\to 0}(\cos(\alpha+\varepsilon) - \cos(\alpha)) = -\varepsilon\sin\alpha. \tag{14}$$

https://doi.org/10.1017/S0263574714000654 Published online by Cambridge University Press

The following relations can be deduced:

$$\begin{aligned}
&\lim_{N\to\infty}\left(\nabla u_k^i\right)^T\left(\prod_{j=i+1}^{N-1}\nabla s_k^j\right)\\
&=\lim_{N\to\infty}\begin{bmatrix}\frac{1}{\Delta\psi_k^i}\left(s\psi_k^{i+1}-s\psi_k^i\right) & -\frac{1}{\Delta\psi_k^i}\left(c\psi_k^{i+1}-c\psi_k^i\right) & 0\\ -\frac{r_k}{\Delta\psi_k^i}\left(s\psi_k^{i+1}-s\psi_k^i\right)+r_k c\psi_{k+1}^i & \frac{r_k}{\Delta\psi_k}\left(c\psi_k^{i+1}-c\psi_k^i\right)+r_k s\psi_{k+1}^i & 1\end{bmatrix}\\
&\quad\times\begin{pmatrix}1 & 0 & r_k\left(c\psi_k^{N-1}-c\psi_k^{i+1}\right)\\ 0 & 1 & r_k\left(s\psi_k^{N-1}-s\psi_k^{i+1}\right)\\ 0 & 0 & 1\end{pmatrix}\\
&=\lim_{N\to\infty}\begin{pmatrix}\frac{1}{\Delta\psi_k^i}\left(s\psi_k^{i+1}-s\psi_k^i\right) & r_k\left(-\frac{1}{\Delta\psi_k^i}\left(s\psi_k^{i+1}-s\psi_k^i\right)+c\psi_k^{N-1}\right)\\ -\frac{1}{\Delta\psi_k^i}\left(c\psi_k^{i+1}-c\psi_k^i\right) & r_k\left(\frac{1}{\Delta\psi_k^i}\left(c\psi_k^{i+1}-c\psi_k^i\right)+s\psi_k^{N-1}\right)\\ 0 & 1\end{pmatrix}^T\\
&=\begin{pmatrix}c\psi_k^i & r_k\left(c\psi_{k+1}-c\psi_k^i\right)\\ s\psi_k^i & r_k(s\psi_{k+1}-s\psi_k^i)\\ 0 & 1\end{pmatrix}^T. \qquad (15)
\end{aligned}$$

Using Assumption 2 and Equation (15), the matrix $Q_k^i$ can be rewritten as follows:

$$\begin{aligned}
Q_k^i&=\lim_{N\to\infty}\left(\prod_{j=i+1}^{N}\nabla s_k^j\right)^T\nabla u_k^i C_{u_k}^i\left(\nabla u_k^i\right)^T\left(\prod_{j=i+1}^{N}\nabla s_k^j\right)\\
&=\begin{pmatrix}c\psi_k^i & r_k\left(c\psi_{k+1}-c\psi_k^i\right)\\ s\psi_k^i & r_k(s\psi_{k+1}-s\psi_k^i)\\ 0 & 1\end{pmatrix}\begin{pmatrix}\delta_{D_k^i}^2 & 0\\ 0 & \delta_{\Delta\psi_k^i}^2\end{pmatrix}\begin{pmatrix}c\psi_k^i & r_k\left(c\psi_{k+1}-c\psi_k^i\right)\\ s\psi_k^i & r_k(s\psi_{k+1}-s\psi_k^i)\\ 0 & 1\end{pmatrix}^T.
\end{aligned}$$

Thus, the elements of matrix $Q_k^i$ can be expressed as follows:

$$Q_{k,11}^i=\sigma_{D_k^i}^2c^2\psi_k^i+\sigma_{\Delta\psi_k^i}^2r_k^2\left(c\psi_{k+1}-c\psi_k^i\right)^2, \qquad (16)$$

$$Q_{k,12}^i=Q_{k,21}^i=\sigma_{D_k^i}^2c\psi_k^is\psi_k^i+\sigma_{\Delta\psi_k^i}^2r_k^2\left(c\psi_{k+1}-c\psi_k^i\right)\left(s\psi_{k+1}-s\psi_k^i\right), \qquad (17)$$

$$Q_{k,13}^i=Q_{k,31}^i=\sigma_{\Delta\psi_k^i}^2r_k\left(c\psi_{k+1}-c\psi_k^i\right), \qquad (18)$$

$$Q_{k,22}^i=\sigma_{D_k^i}^2s^2\psi_k^i+\sigma_{\Delta\psi_k^i}^2r_k^2\left(s\psi_{k+1}-s\psi_k^i\right)^2, \qquad (19)$$

$$Q_{k,23}^i=Q_{k,32}^i=\sigma_{\Delta\psi_k^i}^2r_k\left(s\psi_{k+1}-s\psi_k^i\right), \qquad (20)$$

$$Q_{k,33}^i=\sigma_{\Delta\psi_k^i}^2. \qquad (21)$$

https://doi.org/10.1017/S0263574714000654 Published online by Cambridge University Press

Using Assumption 1, the elements sum of $Q_k^i$ can be rewritten as Riemann integral regarding $\psi_k^i$,

$$\begin{aligned}
Q_{k,11} &= \lim_{N\to\infty}\sum_{i=0}^{N-1} Q_{k,11}^i \\
&= \lim_{N\to\infty}\sum_{i=0}^{N-1}\left[\sigma_{D_k^i}^2 c^2\psi_k^i + \sigma_{\Delta\psi_k^i}^2 r_k^2\left(c\psi_{k+1}-c\psi_k^i\right)^2\right] \\
&= \lim_{N\to\infty}\sum_{i=0}^{N-1}\left|\Delta\psi_k^i\right|\left[c^2\psi_k^i k_D\left|r_k\right| + r_k^2\left(c\psi_{k+1}-c\psi_k^i\right)^2 k_\psi\right] \\
&= sign(\Delta\psi_k)\lim_{N\to\infty}\sum_{i=0}^{N-1}\left[c^2\psi_k^i k_D\left|r_k\right| + r_k^2\left(c\psi_{k+1}-c\psi_k^i\right)^2 k_\psi\right]\Delta\psi_k^i \\
&= sign(\Delta\psi_k)\int_{\psi_k}^{\psi_{k+1}}\left(k_D\left|r_k\right|c^2 x + r_k^2 k_\psi\left(c\psi_{k+1}-cx\right)^2\right)dx \\
&= \frac{1}{2}(k_D\left|r_k\right| + r_k^2 k_\psi)sign(\Delta\psi_k)\left(\Delta\psi_k + \frac{s(2\psi_{k+1})-s(2\psi_k)}{2}\right) \\
&\quad + r_k^2 k_\psi sign(\Delta\psi_k)(\Delta\psi_k c^2\psi_{k+1} - 2c\psi_{k+1}(s\psi_{k+1}-s\psi_k)).
\end{aligned} \tag{22}$$

In the same manner, the other elements of $Q_k$ can be obtained as follows:

$$\begin{aligned}
Q_{k,12} = Q_{k,21} &= -\frac{k_D\left|r_k\right| + r_k^2 k_\psi}{4} sign(\Delta\psi_k)\left(c(2\psi_{k+1}) - c(2\psi_k)\right) + r_k^2 k_\psi sign(\Delta\psi_k) \\
&\quad \times\left(\frac{1}{2}\Delta\psi_k s(2\psi_{k+1}) + c(2\psi_{k+1}) - c(\psi_k+\psi_{k+1})\right),
\end{aligned} \tag{23}$$

$$\begin{aligned}
Q_{k,13} = Q_{k,31} &= r_k k_\psi sign(\Delta\psi_k)(\Delta\psi_k c\psi_{k+1} - s\psi_{k+1} + s\psi_k) \\
&= \left|r_k\right| k_\psi(\Delta\psi_k c\psi_{k+1} - s\psi_{k+1} + s\psi_k),
\end{aligned} \tag{24}$$

$$\begin{aligned}
Q_{k,22} &= \frac{1}{2}(k_D\left|r_k\right| + r_k^2 k_\psi)sign(\Delta\psi_k)\left(\Delta\psi_k - \frac{s(2\psi_{k+1})-s(2\psi_k)}{2}\right) \\
&\quad + r_k^2 k_\psi sign(\Delta\psi_k)(\Delta\psi_k s^2\psi_{k+1} + 2s\psi_{k+1}(c\psi_{k+1}-c\psi_k)),
\end{aligned} \tag{25}$$

$$\begin{aligned}
Q_{k,23} = Q_{k,32} &= r_k k_\psi sign(\Delta\psi_k)(\Delta\psi_k s\psi_{k+1} + c\psi_{k+1} - c\psi_k) \\
&= \left|r_k\right| k_\psi(\Delta\psi_k s\psi_{k+1} + c\psi_{k+1} - c\psi_k),
\end{aligned} \tag{26}$$

$$Q_{k,33} = k_\psi\left|\Delta\psi_k\right|, \tag{27}$$

where $sign(\Delta\psi_k) = sign(r_k) = \left|r_k\right|/r_k \neq 0$.

**2. Straight line motion**

When $r_k \to \infty$, $\nabla\psi_k \to 0$, the trajectory of arc motion turns into a straight line, a special case of arc motion for mobile robots. The variance in change in motion direction satisfies the relation $\delta_{\Delta\psi_k}^2 = k_\psi^D\left|D_k\right| = k_\psi^D\left|r_k\right|\left|\Delta\psi_k\right|$. Satisfying the above same conditions and $N\to\infty$, the followings

https://doi.org/10.1017/S0263574714000654 Published online by Cambridge University Press

can be obtained

$$\psi_{k+1} = \psi_k^i + \frac{N-i}{N}\Delta\psi_k,\ D_k \to \frac{D_k}{N},\ \Delta\psi_k \to \frac{N-i}{N}\Delta\psi_k. \tag{28}$$

Therefore given the conditions (2), (5), (6), (13), (14), and (28), the elements of $Q_k$, (16)–(21), can now be rewritten.

$$\begin{aligned}
\lim_{\substack{N\to\infty, r_k\to\infty \\ D_k = r_k\Delta\psi_k}} Q_{k,11}^i &= k_D\frac{|D_k|}{N}c^2\psi_k + k_\gamma^D\frac{|D_k|}{N}\left(\frac{D_k}{\Delta\psi_k}\right)^2\left(-\frac{N-i}{N}\Delta\psi_k s\psi_k\right)^2 \\
&= k_D\,|D_k|\,c^2\psi_k\frac{1}{N} + k_\psi^D\,|D_k|\,(D_k)^2 s^2\psi_k\frac{(N-i)^2}{N^3} \\
\lim_{\substack{N\to\infty, r_k\to\infty \\ D_k = r_k\Delta\psi_k}} Q_{k,12}^i &= \frac{1}{2}k_D\,|D_k|\,s(2\psi_k)\frac{1}{N} - \frac{1}{2}k_\psi^D\,|D_k|\,(D_k)^2 s(2\psi_k)\frac{(N-i)^2}{N^3} \\
\lim_{\substack{N\to\infty, r_k\to\infty \\ D_k = r_k\Delta\psi_k}} Q_{k,13}^i &= k_\psi^D\frac{|D_k|}{N}\frac{D_k}{\Delta\psi_k}\left(-\frac{N-i}{N}\Delta\psi_k s\psi_k\right) = -k_\psi^D\,|D_k|\,D_k s\psi_k\frac{N-i}{N^2} \\
\lim_{\substack{N\to\infty, r_k\to\infty \\ D_k = r_k\Delta\psi_k}} Q_{k,22}^i &= k_D\,|D_k|\,s^2\psi_k\frac{1}{N} + k_\psi^D\,|D_k|\,(D_k)^2 c^2\psi_k\frac{(N-i)^2}{N^3} \\
\lim_{\substack{N\to\infty, r_k\to\infty \\ D_k = r_k\Delta\psi_k}} Q_{k,23}^i &= k_\psi^D\,|D_k|\,D_k c\psi_k\frac{N-i}{N^2} \\
\lim_{\substack{N\to\infty, r_k\to\infty \\ D_k = r_k\Delta\psi_k}} Q_{k,33}^i &= k_\psi^D\,|D_k|\,\frac{1}{N}.
\end{aligned}$$

Besides when $n \to \infty$ the following derivation can be used according to the limit sums of infinitude function

$$\sum_{x=0}^{n} x = \frac{n(n+1)}{2} \approx \frac{n^2}{2}, \tag{29}$$

$$\sum_{x=0}^{n} x^2 = \frac{n(n+1)(2n+1)}{6} \approx \frac{n^3}{3}. \tag{30}$$

The elements of $Q_k$, (16)–(21) can now be rewritten based on the above equations when $N \to \infty$

$$Q_{k,11} = |D_k|\left(k_D c^2\psi_k + \frac{1}{3}k_\psi^D(D_k)^2 s^2\psi_k\right), \tag{31}$$

$$Q_{k,12} = Q_{k,21} = \frac{1}{2}\,|D_k|\left(k_D - \frac{1}{3}k_\psi^D(D_k)^2\right)s(2\psi_k), \tag{32}$$

$$Q_{k,13} = Q_{k,31} = -\frac{1}{2}k_\psi^D\,|D_k|\,D_k s\psi_k, \tag{33}$$

$$Q_{k,22} = |D_k|\left(k_D s^2\psi_k + \frac{1}{3}k_\psi^D(D_k)^2 c^2\psi_k\right), \tag{34}$$

https://doi.org/10.1017/S0263574714000654 Published online by Cambridge University Press

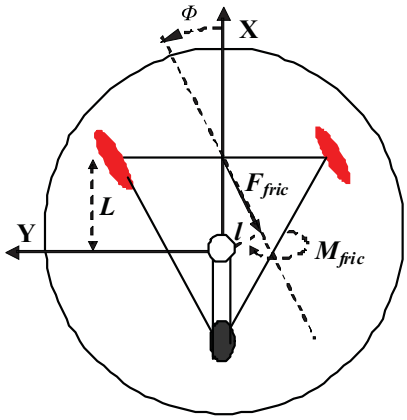



Fig. 2. The orientation change caused by slippage.

$$Q_{k,23} = Q_{k,32} = \frac{1}{2} k_{\psi}^{D} |D_k| D_k c\psi_k, \tag{35}$$

$$Q_{k,33} = k_{\psi}^{D} |D_k| . \tag{36}$$

**3. Rotation on the spot**

When $r_k \to 0$ the curve motion turns into rotation on a certain spot, a special case of arc motion. On the basis of the above derivation, the elements of $Q_k^i$ can be rewritten as follows:

$$Q_{k,11} = Q_{k,12} = Q_{k,21} = Q_{k,22} = Q_{k,13} = Q_{k,31} = 0,$$
$$Q_{k,33} = k_{\psi}^{\psi} |\Delta\psi_k| .$$

Through the above analysis, the non-systematic error can be expressed as a certain function with the odometric control input and the parameters between the ground and the wheels. If the odometric error is compensated for online at the feedback end by modifying odometric input dynamically, the odometric accumulative error decreases in real-time and localisation precision is improved during long-range navigation.

**4. Odometric Systematic Error Analysis**

Systematic error refers to the internal error caused by modelling errors or low precision of odometry. In general, as the fine difference in wheel radius leads to slippage, the accumulative errors occur in the movements. However, the systematic error can be obtained in real time and compensated for by feedback. In most cases, the systematic error incurred from unequal radius on drive wheels draws much attention.

Figure 2 shows a hypothesis that a relative slippage occurs when the robot is moving $\varphi$ means the steer angle, and $\Delta\theta$ denotes the change in orientation. The wheels are mechanically linked, both in translation and in rotation. If there is some slight difference between the radii of both drive wheels slippage occurs. The friction force $F_{\text{fric}}$ between the ground and wheels causes a moment of rotation $M_{\text{fric}}$. Therefore, the rotational moment is given by

$$M_{\text{fric}} = -L \sin\phi \cdot F_{\text{fric}} = -\mu mg \cdot L \sin\phi \propto -\sin\phi, \tag{37}$$

where $\mu$ is the kinetic friction factor. The friction force $F_{\text{fric}}$ depends on the surface properties.

With the law rotation,[15] the following expression can be debuced approximately

$$M_{\text{fric}} = J\alpha K_{\text{rigid}} \Delta\theta,$$

where $k_{\text{rigid}}$ is the rotational rigid factor, $J$ and $\alpha$ are the rotational inertia and angular acceleration.

https://doi.org/10.1017/S0263574714000654 Published online by Cambridge University Press

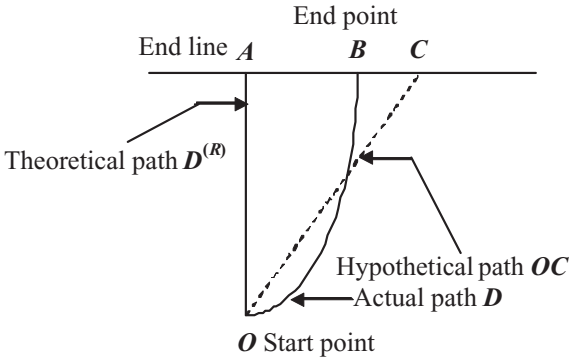



Fig. 3. The distance change caused by fine difference in wheel radius.

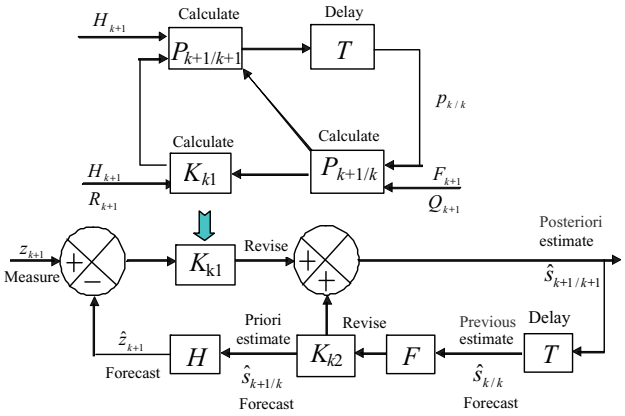



Fig. 4. Flow diagram of pose tracking.

To compensate for the systematic error caused by friction the relation between odometric input and error needs. When relative slippage occurs between the wheel and the ground, the relational expression is obtained from Equation (37)

$$\Delta\theta \propto \eta \sin\phi \ \text{deg/s}\,(\eta < 0). \tag{38}$$

According to the above relations the approximate sine relations are inferred between the steer angle $\varphi$ and the change in orientation $\Delta\theta$, which means the orientation deviation of distance travelled per meter in steer angle direction when the robot makes turns during its motion. The constant $\eta$ depends on the different mechanical structures.

The sketch map in Fig. 3 shows the relation between the actual path $D$ and the theoretical path $D^{(R)}$ for mobile robots. It is supposed that the robot moves along line $OA$ to the end point $A$. The slight difference between drive wheel radii drives the robot away from the straight line $OA$ to point $B$ along the actual path $OB$. Obviously the relation $D > D^{(R)}$ is satisfied. The hypothetical path $OC$ approximates $OB$ when $OB$ is long enough. Therefore, the relation between $OA$ and $OC$ is in approximate direct proportion as the equation: $D = \beta D^{(R)}(\beta > 1)$, As a result, the change of distance travelled is denoted as follows:

$$\Delta D = (\beta - 1)D^{(R)}. \tag{39}$$

## 5. Pose Tracking with Odometric Error Feedback

Based on the functional relationships between the odometric control input and non-systematic error as well as the systematic error, the odometric error for mobile robots can be obtained in real time and compensated for by the dynamic change of odometric input. Figure 4 shows the whole flow diagram of error feedback online, including non-systematic error and systematic error. The pose estimate is

https://doi.org/10.1017/S0263574714000654 Published online by Cambridge University Press

updated according to the sensory information based on the theory of Extended Kalman Filter (EKF). The non-linear kinematic model of pose estimate and the sensory measurement model are given as follows[16–19]

$$s_{k+1} = f(s_k, u_k, w_k, \psi_k), z_k = h(s_k, M, v_k),$$

where $w_k$ and $v_k$, the process noise and measurement noise are assumed to be zero mean and white. That is: $E[w_k] = 0$, $E[w_k w_k^T] = Q_k$, $E[v_k] = 0$, $E[v_k v_k^T] = R_k$, $Q_k$ denotes the input noise covariance, $R_k$ means the measurement noise covariance. $w_k$, $v_k$, and $s_k$ are uncorrelated with each other. $M = \{m^t | t = 1, \ldots, T\}$ is the feature map database. $t$ is the number of the features. $h$ is the measurement function of camera sensors and denotes the vision measurement at pose estimate $s_k$ according to $M$.

The above hypothesis can simplify the computation and has little influence on the actual odometric model. The process of pose tracking for mobile robots includes the following steps based on the EKF theory:

(1) Estimate: forecast priori pose estimate and its covariance according to the previous pose estimate:

Forecast priori pose estimate $\hat{s}_{k+1/k} = f(\hat{s}_{k/k}, u_k, 0)$
Forecast priori pose estimate covariance $P_{k+1/k} = F_{k+1} P_{k/k} F_{k+1}^T + W_{k+1} Q_k W_{k+1}^T$
The Jacobian matrices of function $f$

$$F_{k+1} = \frac{\partial f}{\partial s_{k+1}} |\hat{s}_{k/k}, u_k, 0,$$
$$W_{k+1} = \frac{\partial f}{\partial w_{k+1}} |\hat{s}_{k/k}, u_k, 0.$$

(2) Measure: obtain the innovation measurement error and its covariance according to feature database $M$

Estimate measurement $\hat{z}_{k+1} = h(\hat{s}_{k+1/k}, M, 0)$

Innovation measurement error $v_{k+1} = z_{k+1} - \hat{z}_{k+1}$
Measurement noise covariance $E[v_{k+1} v_{k+1}^T] = R_{k+1}$
Innovation process covariance $C_{k+1} = H_{k+1} P_{k+1/k} H_{k+1}^T + V_{k+1} R_{k+1} V_{k+1}^T$
The jacobian matrices of function $h$

$$H_{k+1} = \frac{\partial h}{\partial s_{k+1}} |\hat{s}_{k+1/k}, M, 0,$$
$$V_{k+1} = \frac{\partial h}{\partial v_{k+1}} |\hat{s}_{k+1/k}, M, 0.$$

(3) Match: judge whether actual measurement and estimate measurement match or not

$$\begin{aligned} G_k &= v_{k+1} C_{k+1} v_{k+1}^T, \\ v_{k+1} C_{k+1} v_{k+1}^T &\leq G_0, \end{aligned} \tag{40}$$

where $G_k$ denotes the Mahalanobis distance between the actual measurement and estimate measurement. $G_0$ determines the threshold. If Equation (40) is satisfied the estimate measurement matches the actual measurement. Otherwise, the matching process is recalculated again.

(4) Update: calculate the odometric error feedback gain and posteriori pose estimate and its covariance:

Non-systematic error feedback gain $K_{k1} = P_{k+1/k} H_{k+1}^T C_{k+1}^{-1}$
Systematic error feedback gain $K_{k2} = s_{k/k}(\Delta D_k^{(R)}, \Delta\theta_k)$, according to Eqs. (38) and (39).
Posteriori estimate covariance update: $P_{k+1/k+1} = (I - K_{k1} H_{k+1}) P_{k+1/k}$
Posteriori estimate update $\hat{s}_{k+1/k+1} = \hat{s}_{k+1/k} + K_{k1} v_{k+1} + K_{k2}$

https://doi.org/10.1017/S0263574714000654 Published online by Cambridge University Press

Table I. The pose estimates of pose tracking based on the odometric error modelling for mobile robots..

| |
|---|
| Input: the previous pose estimate and the control input of odometry |
| Output: the posteriori pose estimate |
| Step 1: initialize $E[s_0] = \hat{s}_0$, $E\left\{(s_0 - \hat{s}_0)(s_0 - \hat{s}_0)^T\right\} = P_0$ |
| For each time $k = 1,...N$, do |
| Step 2: calculate the systematic error feedback gain $K_{k2}$; |
| Step 3: forecast the priori pose estimate $\hat{s}_{k+1/k}$; |
| Step 4: calculate the two jacobian matrices of function $f$, $F_{k+1}$, $W_{k+1}$; |
| Step 5: calculate the non-systematic error covariance matrix $Q_k$; (including circular arc motion and straight line motion) |
| Step 6: forecast the priori pose estimate covariance $P_{k+1/k}$ ; |
| Step 7: obtain the pose estimate measurement measured by sensors $\hat{z}_{k+1/k}$; |
| Step 8: calculate the actual sensor measurement $z_{k+1}$; |
| Step 9: calculate the two Jacobian matrices of function $h$, $H_{k+1}$, $V_{k+1}$; |
| Step 10: calculate the innovation measurement error $v_{k+1}$; |
| Step 11: calculate the measurement noise covariance $R_{k+1}$; |
| Step 12: calculate the innovation process covariance $C_{k+1}$; |
| Step 13: calculate the Mahalanobis distance $G_k$; |
| If the matching condition is satisfied, turn to step 14 or Step 2; |
| Step 14: calculate the non-systematic error feedback gain $K_{k1}$; |
| Step 15: update priori pose estimate covariance $P_{k+1/k+1}$; |
| Step 16: update priori pose estimate $s_{k+1/k+1}$; |
| End For |



(A) ERSP/SCORPION (B) HIT-3SDR (C) Pioneer3-DX

Fig. 5. The different driving-type robots.

The whole process is expressed as the following Table I according to Fig. 4.

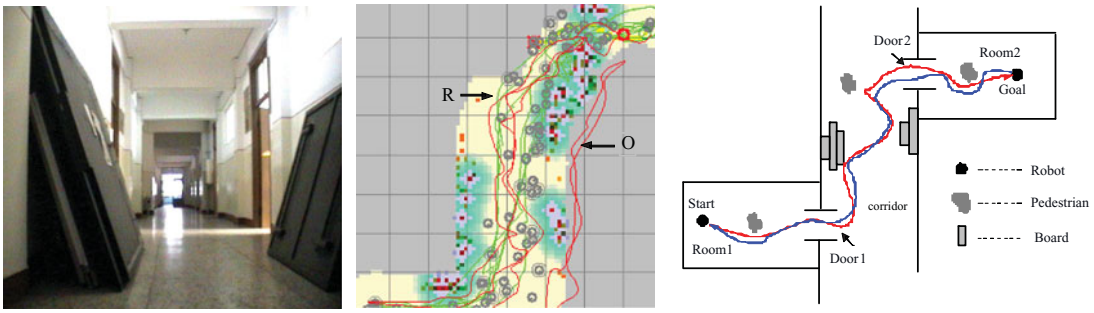
## 6. Experiment and Analysis

### *6.1. Test platform and autonomous navigation*

To test that the algorithm of pose tracking with error feedback in real time is applicable and efficient for the differential drive or synchronous-drive mobile robots, localisation experiments have been done on these two types of mobile robots in indoor environments. As is shown in Fig. 5(a), the typical robot is the differential drive mobile robot, ERSP/SCORPION. This robot is equipped with a web camera mounted on the top, an array of IR sensors around the body to measure the distance from an obstacle, and a bump sensor in front of the body to detect the obstacles. The robot gathers the data from the onboard sensors to build occupancy grid map and locate itself in the global environment.

As the path of Fig. 6(c) shows, ERSP is driven to move away from a room using a joystick first along the corridor, enters another room, then returns to the starting point by the same path for a few successive times. At the same time, the landmarks created by the camera are built and saved in the database. The poses of the landmarks have been expressed in a global reference frame. After building

https://doi.org/10.1017/S0263574714000654 Published online by Cambridge University Press




A: Navigation Environment B: Occupancy grid map C: Navigation path

Fig. 6. The simultaneous localisation and mapping.

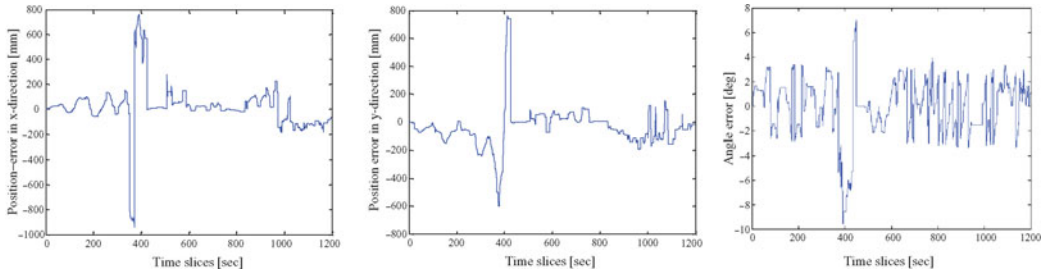



Fig. 7. Position error in XY direction and angle error by the odometer.

the initial environment map, the robot begins exploring the area according to the initial map for about 20 min from the starting point. During autonomous exploration, the initial map keeps updating continuously with respect to the detected new obstacles. The robot locates itself in the global map by the landmarks. If the goal is set, the robot chooses the shortest path to reach the goal. Figure 6(a) shows the scene of the corridor in the testing path. Figure 6(a) gives the occupancy grid map relative to the scene in Fig. 6(c). The dynamic occupancy grid map is updated according to such data as camera, infrared finder and bumper. The darkness of colour denotes the possibility of obstacles. The darker the colour is, the more likely the obstacle is. It is also shown that the path of odometry $O$ is not the same as the robot path $R$. It is because that the odometric error (non-systematic or systematic error) results in the increasing of accumulative errors significantly, and gives rise to the odometric error "drift" after long-term navigation.

### *6.2. Odometric error modelling*

**Non-systematic error modelling**: The wheel encoder mounted at each wheel records the raw odometer revolutions and returns the pose of robot at each time step in the true tests at the beginning of navigation. Along with the increase of navigation distance, the odometric encorder error is gradually increasing. The vision is used to obtain pose estimates to revise the odometric error by matching current information with landmarks (by observation of the environment or from a-priori information). Therefore, the pose or angle component of an odometric error is computed as difference between the estimate from the EKF and the vision localisation. Figure 7 illustrates the odometric pose error (position error and angle error) when ERSP navigates for 20 min in the scene of Fig. 6(c). As is shown in Fig. 7, the pose error is smaller at the beginning of the navigation. With the increase of movement distance, the pose error of the robot is growing. When the robot moves to a pile of obstacles in the corridor at the 350th second, collision and sideslip occur. The odometric accumulative error of the robot is growing significantly and pose error has a big fluctuation. At the time, the "kidnapping" happens. The robot abandons locating itself with the odometer. The localisation is realized by its own vision. The vision localisation can efficiently help to reduce odometric accumulative error caused by long-range navigation. The visual accuracy can reach to more than 76% when the position error in XY direction is smaller than 50 cm. The robot takes the images continuously, from which the SIFT features are extracted, and matches with the landmarks in the database. If some successful matches happen, the robot uses the matched landmarks to relocate itself and shake off "kidnapping"

https://doi.org/10.1017/S0263574714000654 Published online by Cambridge University Press

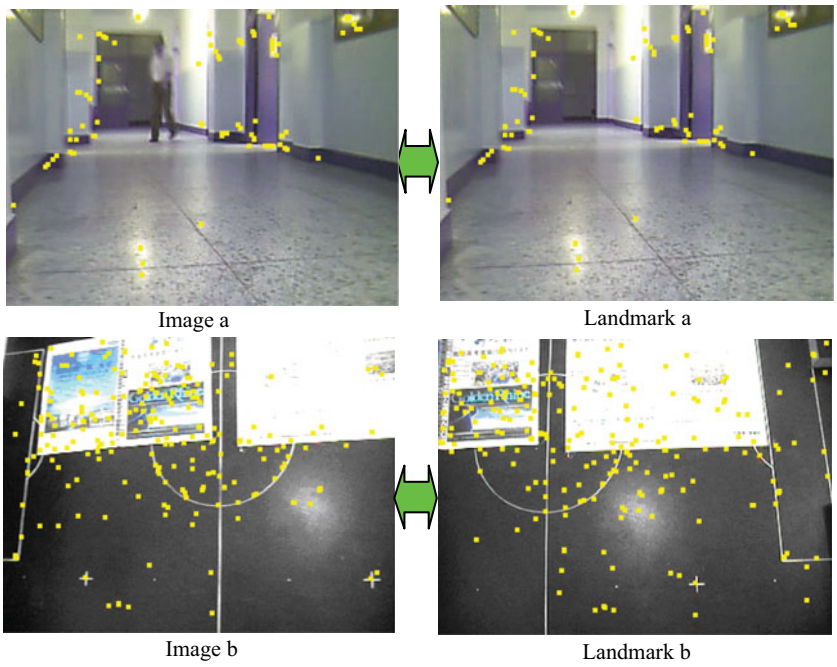



Fig. 8. The **SIFT** feature extraction and match between the current image and the landmarks in the database.

quickly in the new environment. Figure 8 shows that the process of feature extraction and match between the current image and the landmarks. Image (a) is taken in the corridor by the camera, and landmark (a) is its corresponding landmark in the database. The extracted SIFT features from Image (a) and Landmark (a) are 247 and 223, respectively, and the successful match features are 103, and the matching time is 234 ms. Image (b) is taken in front of a pile of boards in the corridor. The SIFT features from Image (b) and Landmark (b) are 540 and 401, respectively, the successful match features are 224, and the matching time is 362 ms. After localisation and mapping for about 100 s, the robot relocates itself in the new environment again according to these landmarks, such as Landmark (a) or Landmark (b), updates the odometer data by vision localisation, the occupancy grid map is updated again, and enters into autonomous navigation at the 450th second time slice. The pose error is growing smaller and fluctuates steadily. The "kidnapping" is over. The average pose error for the whole navigation is given as follows:

$$d_{\text{mean}} = \sqrt{\Delta x^2 + \Delta y^2} = 124.0137\,\text{mm}, \Delta\theta_{\text{mean}} = 3.8842^\circ$$

Figure 9 compares three localisation methods, such as the EKF methods, the EKF method after odometric non-systematic error modelling (EMEKF) and Monte Carlo Localisation (MCL) method. MCL algorithm represents the classical localisation by a set of weighted hypotheses (samples), which approximate the posterior under a common Bayesian formulation of the localisation problem. The number of chosen samples affects the localisation precision with MCL remarkably. The localisation precision improves with the increase of the number of the samples. However, more samples cost much more computational time. 50 samples are used in this location test. The average position error and angle error of MCL is 472.32 mm and 6.81°. The localisation precision of MCL is higher than that of EKF, and is lower than that of EMEKF obviously. The pose error and angle error of EMEKF are reduced by 70.37% and 66.89% compared with that of MCL, respectively. It also shows that the localisation error of EMEKF is much less than that of EKF. The position error and the angle error are reduced by 80.49% and 81.31% compared with that of EKF, respectively. In the whole process, the parameters, $k_D, k_\psi, k_\psi^\psi, k_\psi^D$, are set as 0.89, 1.48, 0.33, 0.23, respectively when $r_k = 5$ m in the following experimental test. Therefore, the non-systematic error feedback in real time can reduce the

https://doi.org/10.1017/S0263574714000654 Published online by Cambridge University Press

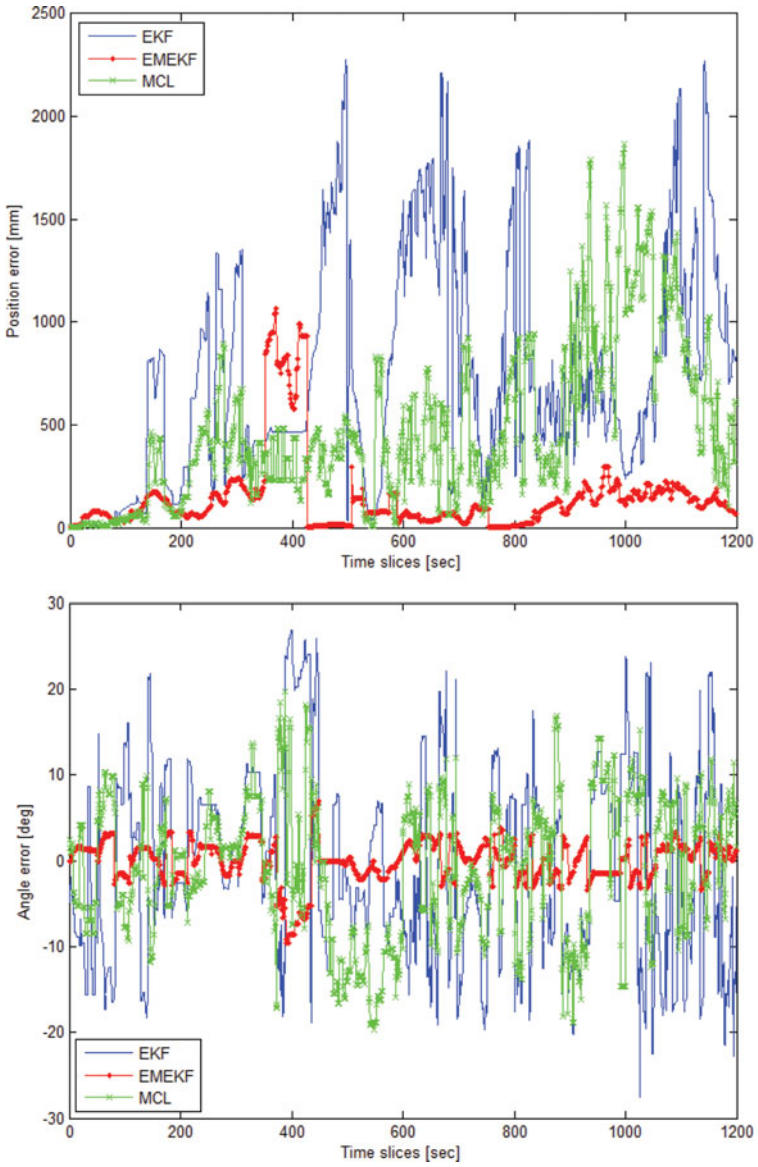



Fig. 9. The position error and angle error before and after odometric non-systematic error modelling during pose tracking.

localisation error efficiently and improve the accuracy of localisation during autonomous navigation for mobile robots.

**Systematic error modelling**: Table II shows the measurement data when ERSP is driven forward about 10 m for 11 times. $\theta_{\text{Start}}$ is the initial angle of movements $\varphi$ and $\nabla\theta$ are the steer angle and angle error. Then the actual distance $D$ and the measurement value $D^{(R)}$ are used to obtain the scaling factor $\beta = D/D^{(R)}$. The mean of scaling factor is $\beta \approx 1.0013$. In the same scene, the data for a synchronous drive robot HIT-3SDR, as shown in Fig 5(b), satisfies $\beta \approx 1.0027$. Therefore, the distance deviation caused by tiny differentia of radii exists in both synchronous drive and differential drive mobile robots generally. The systematic error has correlation with the control input of odometry and can be compensated for at the feedback end of control system.

According to the data in Table II, the sampling curve and fitting curve in the same scene for different driving type mobile robots are drawn in Fig. 10. The red solid line and dashed line represent the sampling curve and fitting curve for ERSP and the green lines show the data for HIT-3SDR. So the relation between $\varphi$ and $\Delta\theta$ for ERSP can be given as the expression: $\Delta\theta \approx -2.23\sin\varphi$(deg/s); the

https://doi.org/10.1017/S0263574714000654 Published online by Cambridge University Press

Table II. The distance and angle error with different initial angle along the same direction.

| Initial angle $\theta_{Start}$/(deg) | Actual distance $D$/(mm) | Measurement distance $D^{(R)}$/(mm) | Ratio of distance $D/D^{(R)}$ | Steer angle $\varphi$/(deg) | Angle error $\Delta\theta$/(deg) |
|---|---|---|---|---|---|
| 7.9 | 9825.4 | 9815.6 | 1.000998 | 82.1 | −2.3 |
| 40.5 | 9887.6 | 9874.3 | 1.001467 | 49.5 | −1.4 |
| 78.8 | 9858.4 | 9836.2 | 1.001347 | 14.2 | −0.3 |
| 103.4 | 9734.6 | 9726.9 | 1.002257 | −18.4 | 0.8 |
| 133.0 | 9785.5 | 9773.7 | 1.000792 | −43.0 | 1.2 |
| 163.3 | 9778.9 | 9767.8 | 1.001207 | −73.3 | 1.8 |
| 192.3 | 9956.5 | 9946.8 | 1.001136 | −102.3 | 1.9 |
| 212.6 | 9946.9 | 9931.5 | 1.000975 | −122.6 | 2.1 |
| 249.7 | 9978.9 | 9968.3 | 1.001551 | −159.7 | 0.8 |
| 305.5 | 9875.4 | 9856.7 | 1.001063 | −215.5 | −0.5 |
| 340.5 | 9830.1 | 9815.7 | 1.001897 | −250.5 | −1.8 |

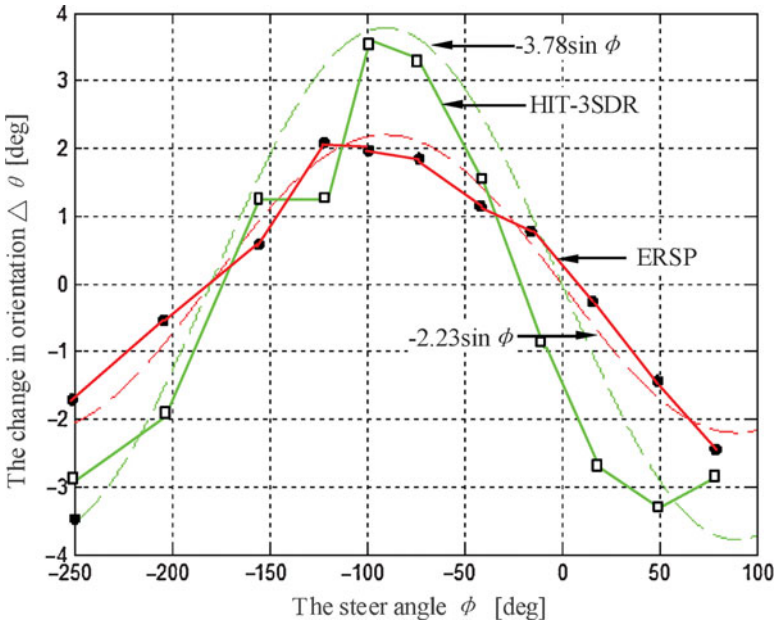



Fig. 10. The relations between $\Delta\theta$ and $\varphi$.

relation for HIT-3SDR is obtained as: $\nabla\theta \approx -3.78\sin\varphi$(deg/s). Therefore, the angle error generated from the difference in wheel radius has the approximate sine functional relation with the steer angle $\varphi$. The angle error $\Delta\theta$ caused by tiny differentia of radius exists in both synchronous drive and differential drive mobile robots generally and can also be compensated for by changing the odometric control input $\varphi$ in real time.

In this paper, the systematic error has also been compensated for at the end of motion control in real time. Figure 11 shows the discrete data samples when ERSP moves about 10 m in different direction. The precision of localisation data has improved by more than 50% from Fig. 11. The position error has decreased by 73.66% and the angle error by 63.53%. So the systematic error feedback in real time prevents the odometric accumulative error from increasing quickly and improves the pose stability for mobile robots.

The contrast test, UMBmark, is introduced to measure odometric systematic error for different drive mobile robots too. The distribution of Cartesian offsets after the completion of $D = 4\text{m}^2$ path for 5 runs in each sense (clockwise and counter-clockwise), before and after calibration, are shown for different drive platform in Table III. The absolute offsets of the two centres of gravity from the origin are denoted as $r$cw and $r$ccw and are given as follows:

$$r_{cw} = \sqrt{(x_{cw})^2 + (y_{cw})^2}, \quad r_{ccw} = \sqrt{(x_{ccw})^2 + (y_{ccw})^2}.$$

https://doi.org/10.1017/S0263574714000654 Published online by Cambridge University Press

Table III. Key results before and after calibration in the UMBmark test for different drive robots.

| | Differential drive (ERSP) | | Synchronous drive (HIT3-SDR) | |
|---|---|---|---|---|
| UMBmark test | Before calibration | After calibration | Before calibration | After calibration |
| $x_{ccw}$ (mm) | 88 | −34 | 45 | 27 |
| $y_{ccw}$ (mm) | 94 | 42 | 58 | 22 |
| $x_{cw}$ (mm) | 44 | 23 | 92 | −32 |
| $y_{cw}$ (mm) | 55 | 19 | 86 | −36 |
| $E_{max}$ (mm) | 129 | 54 | 126 | 49 |

Table IV. The localisation precision before and after non-systematic and systematic error feedback for different drive mobile robots..

| | | Differential drive mobile robots | | | Synchronous drive |
|---|---|---|---|---|---|
| Odometric error | Mean error (%) | ERSP | Pioneer 3-DX | Pioneer 3-AT | HIT-3SDR |
| Non-systematic error | Angle (deg) | 81.31 | 65.19 | 56.77 | 76.43 |
| | Pose (mm) | 80.49 | 74.21 | 60.23 | 75.64 |
| Systematic error | Angle (deg) | 63.53 | 55.89 | 42.12 | 53.24 |
| | Pose (mm) | 73.66 | 64.21 | 53.66 | 70.51 |

The larger value, $E_{\max}$, between $r_{\text{cw}}$ and $r_{\text{ccw}}$, is defined as the measure of odometric accuracy for systematic errors.

$$E_{\max} = \max(r_{\text{cw}}, r_{\text{ccw}}).$$

The systematic error is about 54 mm for the differential drive robot ERSP in UMBmark test, and it is about 49 mm for a synchronous drive robot HIT-3SDR. Therefore, the systematic error is far more than the average pose error (position error = 7.36 mm, angle error = 0.67°) after systematic error modelling. In addition, the UMBmark method can not be acquired and compensated in real time using input of odometry (velocity or angular velocity). Therefore, it is not often used to compensate systematic error in larger autonomous navigation.

**Localisation precision and computational efficiency of odometric error model**: Localisation experiments before and after odometric error feedback were carried out for differential drive and synchronous drive mobile robots. As is shown in Table IV, the localisation precision has been improved greatly for different drive mobile robots. Therefore, the pose tracking algorithms with odometric error feedback online is feasible and efficient during the long-range navigation for mobile robots. The method can map the uncertain non-systematic error $Q_k$ or systematic error (distance deviation $\nabla D$ *or* angle deviation $\nabla\theta$) into the control input of odometry $u_k(D^{(R),}\varphi)$. The control system obtains the compensation by adjusting the non-systematic error gain $K_{k1}$ or systematic error gain $K_{k2}$ effectively. Therefore, it denotes that odometric error can be obtained and compensated for in real time at the feedback control end. The method of odometric error modelling in real time reduces the intrinsic or extrinsic accumulative error during autonomous navigation and improves the localisation accuracy.

Figure 12 shows the localisation time for three localisation methods, EKF methods, the EKF after odometric error modelling (EMEKF) and Monte Carlo Localisation (MCL) method, with a total of 88 times near the landmarks. Fifty samples are used with MCL in the above localisation scene. The localisation time of MCL, 898.65 ms, is the longest among three localisation methods in the test. Because the particle degeneration often happens in traditional Monte Carlo method, re-sampling for the degenerative particles has to be used, in which case it costs much computational time in the process of iterative operation. It also shows the localisation time of both localisation methods based on EKF is similar. The average time of EKF is 579.21 ms. It is 659.25 ms for EMEKF. The localisation time increases by 12.14%. It is because it takes time to calculate the error gains and Jacobian matrices repeatedly in the process of odometric error feedback. However though the whole localisation process sacrifices a little time cost which increases by 12.14%, a higher localisation precision is achieved.

https://doi.org/10.1017/S0263574714000654 Published online by Cambridge University Press

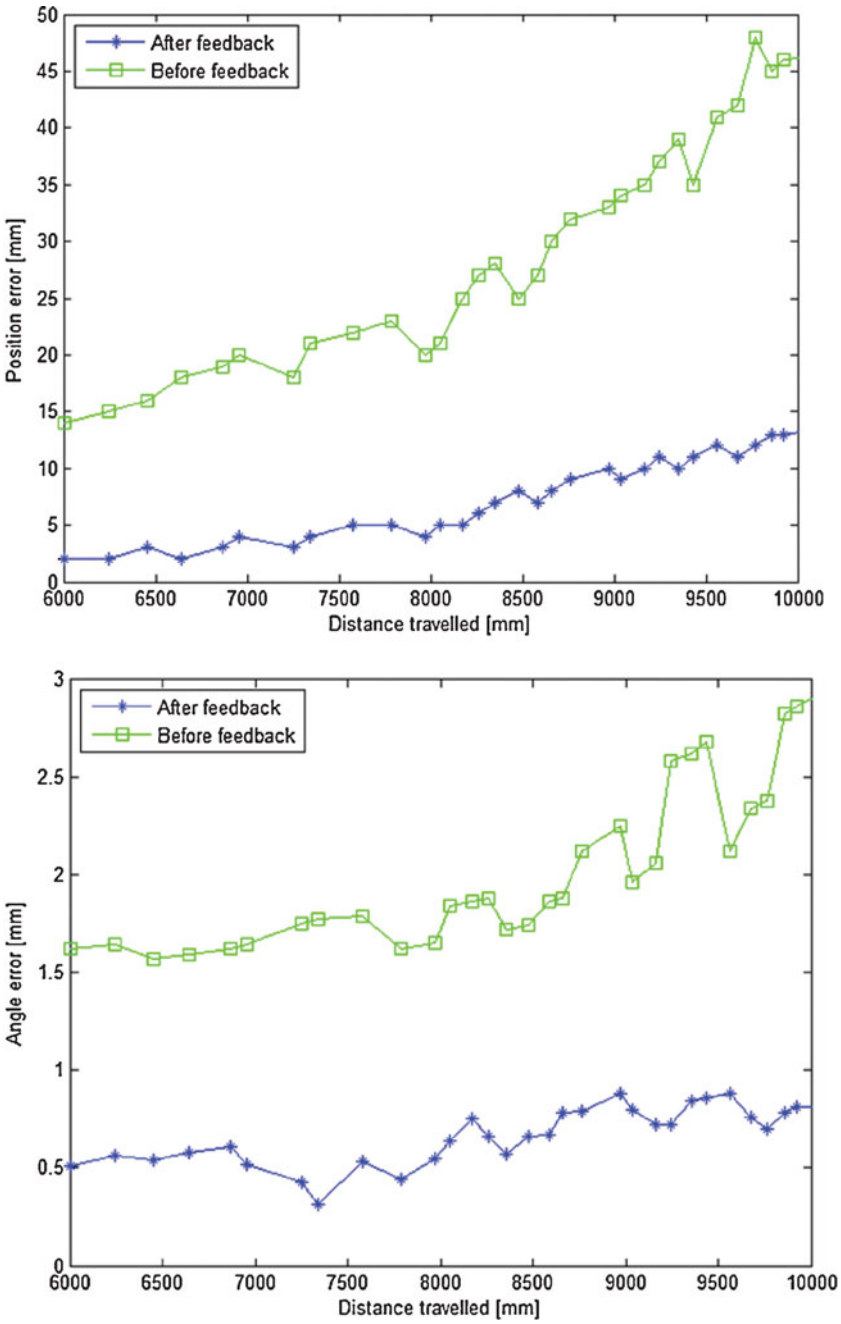



Fig. 11. The position and angle error before and after odometric systematic error modelling during pose tracking.

The position error and the angle error decreases by 80.49% and 81.31%, respectively. In terms of the return on investment in economics, it is quite necessary to adopt odometric error feedback in real-time for mobile robots during long-range navigation.

## 7. Conclusion

In this paper, we analyse odometric error modelling for different driving type mobile robots. A general approach to odometric error modelling is proposed with respect to both synchronous drive roller robot and differential drive roller robot. The method presents a hypothesis that the robot path approximates circular arcs. The approximate function relationships between the control input of odometry and non-systematic error as well as systematic error are based on the odometric error propagation law.

https://doi.org/10.1017/S0263574714000654 Published online by Cambridge University Press

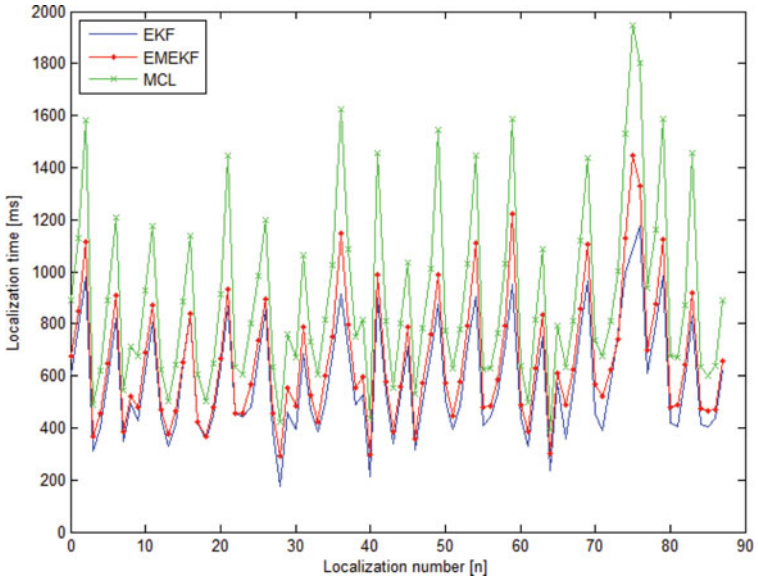



Fig. 12. The localisation time before and after error feedback.

Further, a new pose keeping algorithm for mobile robot is proposed in this paper, which is used online to obtain and reduce non-systematic error and systematic error of the odometry during long-range movements. The experiments denote that the algorithm decreases the accumulative error of odometry efficiently, and improves pose precision significantly during pose tracking for different drive mobile robots. Therefore, when the physical constraints of robot are considered, the algorithm of pose tracking with odometric error feedback in real time can be applied to other drive type mobile robots, such as all-wheel-drive or autonomous vehicles which will be main research direction for the future.

**Acknowledgements**

This work is partially supported by the National Natural Science Foundation of China (61202376,61374039) and the key nurture discipline of Shanghai Second Polytechnic University (Management Science and Engineering) (XXKPY1313). And it is also supported by Innovation Program of Shanghai Municipal Education Commission (13ZS137,13YZ075). Thanks for the help.

**References**

1. J.-D. Yang, J.-H. Yang and B.-R. Hong, "An efficient approach to odometric error modeling for mobile robots," *Acta Autom. Sin.* **35**(2), 168 (2009).
2. G. Antonelli and S. Chiaverini, "Linear estimation of the physical odometric parameters for differential-drive mobile robots," *Auton. Robots* **23**(1), 59–68 (2007).
3. G. Antonelli and S. Chiaverini, "Linear Estimation of the Odometric Parameters for Differential-Drive Mobile Robots," *2006 IEEE/RSJ International Conference on Intelligent Robots and Systems*, Beijing, PRC (Oct. 2006) pp. 3287–3292.
4. A. Korodi and T. L. Dragomir, "Correcting Odometry Errors for Mobile Robots Using Image Processing," *Proceedings of the International MultiConference of Engineers and Computer Scientists (IMECS 2010)* Vol II, Hong Kong (Mar. 17-19, 2010).
5. D. Graovac, S. Juriü-Kavelj and I. Petrović, "Mobile robot pose tracking by correlation of laser range finder scans in Hough domain," *IEEE 19th International Workshop on Robotics in Alpe Adria Danube Region RAAD* , IEEE, Issue 2 (2010) pp. 273–278
6. A. Rusdinar, J. Kim and S. Kim, "Error pose correction of mobile robot for SLAM problem using laser range finder based on particle filter," *System* **200**, 52–55 (2010).
7. K. S. Chong and L. Kleeman, "Feature-based mapping in real, large scale environments using an ultrasonic array," *Int. J. Robot. Res.* **18**(1), 3–19 (1999).
8. K. S. Chong and L. Kleeman, "Accurate Odometry and Error Modeling for a Mobile Robot," *International Conference on Robotics and Automation*, vol. 4 (1997) pp. 2783–2788.
9. A. Martinelli, "State estimation based on the concept of continuous symmetry and observability analysis: The case of calibration," *IEEE Trans. Robot. - TRob* **27**(2), 239–255 (2011).

https://doi.org/10.1017/S0263574714000654 Published online by Cambridge University Press

10. A. Martinelli,"Using the Distribution Theory to Simultaneously Calibrate the Sensor of a Mobile Robot," *Robotics Science and Systems (RSS'09)*, Seattle, USA (2009).
11. M. Josep, L.G. Jose and A. B. Carlos., "A closed-form expression for the uncertainty in odometry position estimate of an autonomous vehicle," *IEEE Trans. Robot.* **21**(5), 345–401 (2005).
12. J. M. M. Tur, C. Albores-Borja and J. L. Gordillo, "Erratum to: A closed-form expression for the uncertainty in odometry position estimate of an autonomous vehicle," *IEEE Trans. Robot.* **23**(6), 1302 (2007).
13. A. Martinelli, N. Tomatis and R. Siegwart, "Simultaneous localization and odometry self calibration for mobile robot," *Auton. Robot* **22**, 75–85 (2007).
14. P. Jensfelt and H. I. Christensen, "Pose tracking using laser scanning and minimalistic environmental models," *IEEE Trans. Robot. Autom*. **17**(2), 138–147 (2001).
15. T. R. Kane and D. A. Levinson, *Dynamics, Theory and Applications* (McGraw-Hill, NY, 2005).
16. R. Havangi, M. A. Nekoui and M. Teshnehlab, "Adaptive neuro-fuzzy extended kalman filtering for robot localization," *Int. J. Comput. Sci.* **7**(2), 15–23 (Mar. 2010).
17. M. Tur and J. Maria, "Onto Computing the Uncertainty for the Odometry Pose Estimate of a Mobile Robot," *12th IEEE International Conference on Emerging Technologies and Factory Automation*, Patras, Greece (2007) pp. 1340–1345.
18. O. A. Stepanov, V. A. Vasiliev and A. V. Osipov, "Fuzzy and Bayesian algorithms for a nonlinear navigation estimation problem," *Gyroscopy Navig.* **1**(4), 272–278 (2010).
19. O. Bittel and M. Blaich, "Mobile Robot Localization Using Beacons and the Kalman Filter Technique for the Eurobot Competition. Proceedings," *Research and Education in Robotics - EUROBOT 2011. Communications in Computer and Information Science Volume 161 2011. International Conference*, Prague, Czech Republic (Jun. 15–17, 2011).

https://doi.org/10.1017/S0263574714000654 Published online by Cambridge University Press